

G-Transformer: Counterfactual Outcome Prediction under Dynamic and Time-varying Treatment Regimes

Hong Xiong

Harvard University

Cambridge, MA, USA

HONGXIONG@HSPH.HARVARD.EDU

Feng Wu

Massachusetts Institute of Technology

Cambridge, MA, USA

WUFENG@MIT.EDU

Leon Deng

Massachusetts Institute of Technology

Cambridge, MA, USA

LYDENG@MIT.EDU

Megan Su

Massachusetts Institute of Technology

Cambridge, MA, USA

MEGANSU@MIT.EDU

Li-wei H Lehman

Massachusetts Institute of Technology

Cambridge, MA, USA

LILEHMAN@MIT.EDU

Abstract

In the context of medical decision making, counterfactual prediction enables clinicians to predict treatment outcomes of interest under alternative courses of therapeutic actions given observed patient history. Prior machine learning approaches for counterfactual predictions under time-varying treatments focus on static time-varying treatment regimes where treatments do not depend on previous covariate history. In this work, we present G-Transformer, a Transformer-based framework supporting g-computation for counterfactual prediction under dynamic and time-varying treatment strategies. G-Transformer captures complex, long-range dependencies in time-varying covariates using a Transformer architecture. G-Transformer estimates the conditional distribution of relevant covariates given covariate and treatment history at each time point using an encoder architecture, then produces Monte Carlo estimates of counterfactual outcomes by simulating forward patient trajectories under treatment strategies of interest. We evaluate G-Transformer extensively using two simulated longitudinal datasets from mechanistic models, and a real-world sepsis ICU dataset from MIMIC-IV. G-Transformer outperforms both classical and state-of-the-art counterfactual prediction models in these settings. To the best of our knowledge, this is the first Transformer-based architecture for counterfactual outcome prediction under dynamic and time-varying treatment strategies. Code will be released upon publication of the paper.

1. Introduction

Clinicians often have to choose among multiple treatment options for their patients but do not have the ability to test every strategy before making a decision. Counterfactual

prediction in medical decision-making involves the estimation of potential future trajectories of covariates of interest under alternative courses of action given observed history.

Treatment strategies of interest are typically *time-varying*, indicating decisions span multiple time points, and *dynamic*, implying that each treatment decision at a given time point is influenced by the preceding history up to that point. In selecting among competing dynamic treatment strategies, it is useful to obtain counterfactual predictions regarding a patient’s probability of experiencing adverse outcomes under each alternative strategy, based on their observed covariate history. Recent works presented deep learning approaches to estimate time-varying treatment effects (Lim et al., 2018; Bica et al., 2020a,b; Melnychuk et al., 2022) . However, most previous approaches focus on estimating counterfactual outcomes under static time-varying treatment strategies where treatments are not dependent on past covariate history.

In this work, we present G-Transformer, a transformer-based (Vaswani et al., 2017) framework for counterfactual prediction under *dynamic* and *time-varying* treatment strategies. G-Transformer supports g-computation, a causal inference technique for estimating treatment effects under dynamic treatment regimes (Robins, 1986, 1987). G-Transformer estimates the conditional distribution of relevant covariates given covariate and treatment history at each time point using an encoder architecture, then produces Monte Carlo estimates of counterfactual outcomes by simulating forward patient trajectories under treatment strategies of interest. We evaluated G-Transformer extensively using multiple simulated datasets from two mechanistic models where ground-truths under the counterfactual strategies can be measured, and a real-world sepsis dataset to assess G-Transformer’s potential clinical utility in counterfactual predictions under alternative dynamic fluid administration regimes. Our contributions are the following:

- G-Transformer architecture. We introduce a novel Transformer-based architecture that enables counterfactual predictions under dynamic and time-varying treatment strategies to provide estimates of individual or population-level treatment effects. We present a custom sequential training procedure for supporting g-computation that performs better than the seq2seq training typically used in Transformers.
- Evaluation under static time-varying treatment regimes. Using a simulated tumor growth dataset, we demonstrated that G-Transformer out-performed other state-of-the-art deep learning approaches, including rMSN (Lim et al., 2018), CRN (Bica et al., 2020a), G-Net (Li et al., 2021), and Causal Transformer (Melnychuk et al., 2022), in counterfactual prediction under static time-varying treatments, in which treatments are time-varying but do not depend on past covariate history.
- Evaluation under *dynamic* and *time-varying* treatment regimes. We used CVSim (Heldt et al., 2010), a mechanistic model of the cardiovascular system, to simulate counterfactual patient trajectories under various *dynamic* fluid and vasopressor administration strategies, and demonstrated that G-Transformer out-performed other baselines, including G-Net and a linear implementation of g-computation, in counterfactual prediction under dynamic and time-varying treatment regimes.
- Evaluation under real-world ICU dataset. Using real-world data of a sepsis cohort from the MIMIC-IV database (Johnson et al., 2023b), we evaluated the performance

of G-Transformer in predicting outcomes under observational treatment regimes, and demonstrated that G-Transformer can generate clinically meaningful counterfactual predictions under alternative dynamic fluids administration regimes.

Generalizable Insights about Machine Learning in the Context of Healthcare

Our extensive experiments show strong empirical performance of G-Transformer under both static and dynamic time-varying treatment strategies over other state-of-the-art techniques. G-Transformer can facilitate treatment decision making at individual patient level by estimating patient trajectories under different treatment strategies of interest. At a population health level, G-Transformer can potentially be used to estimate population-level treatment effects to inform clinical guidelines and health policies. Although we focus on applications in healthcare in this proposed work, the G-Transformer architecture can be applied to other sequential decision making tasks that involve dynamic and time-varying interventions.

2. Related Work

Recent works by [Lim et al. \(2018\)](#); [Bica et al. \(2020a,b\)](#) presented deep learning approaches to estimate time-varying treatment effects. [Bica et al. \(2020a\)](#) applied ideas from domain adaptation to estimate treatment effects over time while [Lim et al. \(2018\)](#) used RNN regression models with history adjusted marginal structural models (MSMs) ([Van der Laan et al., 2005](#)) to make counterfactual predictions. Causal Transformer (CT) has recently been proposed a Transformer-based architecture to estimate counterfactual outcomes ([Melnychuk et al., 2022](#)). However, previous approaches focus on estimating counterfactual outcomes under time-varying treatment strategies where treatments are not dependent on past covariate history. None of these approaches are designed to estimate effects under *dynamic* treatment strategies, in which treatment depends on recent covariate history. In contrast, our work focus on estimating treatment effects under *dynamic* treatment strategies, in which treatments depend on covariate history.

Dynamic-MSMs can be used to estimate expected counterfactual outcomes under restricted classes of simple dynamic treatment regimes ([Orellana et al., 2010](#); [Shahn et al., 2020](#)). It performs time-varying confounding adjustment via inverse probability weighting. The limitation with dynamic-MSMs is that the optimal treatment strategy of realistic complexity may not be included in the restricted class considered.

G-computation can be used to estimate the average effect of a dynamic treatment regime (DTR) on the population, or the conditional effect given observed patient history. Previous implementations of g-computation used classic linear models ([Taubman et al., 2009](#)) or recurrent neural networks based architectures, such as LSTM ([Li et al., 2021](#)). G-Net ([Li et al., 2021](#)) is based on g-computation and used LSTMs for counterfactual prediction of time-varying treatment outcomes under alternative dynamic treatment strategies. In contrast, our work focused on a Transformer-based architecture to better capture complex dependencies in time-varying data. DeepACE ([Frauen et al., 2023](#)) is a recurrent neural network based model that leverages the g-computation framework to address time-varying confounding, but primarily focuses on estimating the Average Causal Effect (ACE).

Recent work by [Wu et al. \(2023\)](#) presented an alternating sequential model that used Transformers for clinical treatment outcome prediction, but their work did not support

counterfactual prediction. [Seedat et al. \(2022\)](#) and [Holt et al. \(2024\)](#) focused on Continuous-Time Modeling, attempting to predict counterfactual treatment effects over irregular time lengths. They utilized neural controlled differential equations to model patient historical trajectories and attempted to make uncertainty estimates based on this model. T4 ([Liu et al., 2023](#)) introduced a LSTM-based neural network architecture for predicting the counterfactual treatment effects of sepsis. They also estimated the uncertainty associated with treatment effects.

3. Methods

3.1. Background: G-computation and Problem Setup

G-computation [Robins \(1986\)](#) can be used to estimate the average effect of a dynamic treatment regime (DTR) on the population, or the conditional effect given observed patient history. In the latter case, we can estimate the expected counterfactual trajectory of outcomes of interest under alternative treatment strategies of interest for a particular patient history.

Problem Setup Our goal is to predict patient outcomes under alternative future treatment strategies given observed patient histories. We follow notations introduced in [Li et al. \(2021\)](#) in this study.

Let:

- $t \in \{0, \dots, K\}$ denote time, assumed discrete, with K being the end of followup;
- A_t denote the observed treatment action at time t ;
- Y_t denote the observed outcome at time t
- L_t denote a vector of covariates at time t that may influence treatment decisions or be associated with the outcome;
- \bar{X}_t denote the history X_0, \dots, X_t and \underline{X}_t denote the future X_t, \dots, X_K for arbitrary time varying variable X .

At each time point, we assume the causal ordering (L_t, A_t, Y_t) , i.e. the treatments are administered after having observed the covariates at time step t . Let $H_t \equiv (\bar{L}_t, \bar{A}_{t-1})$ denote patient history preceding treatment at time t . A dynamic treatment strategy g is a collection of functions $\{g_0, \dots, g_K\}$, one per time point, such that g_t maps H_t onto a treatment action at time t . An example dynamic strategy might be to administer treatment A if the patient's vital signs, e.g. arterial blood pressure, drops below certain threshold.

Let $Y_t(g)$ denote the counterfactual outcome that would be observed at time t , had treatment strategy g been followed from baseline ([Robins, 1986](#)). Further, let $Y_t(\bar{A}_{m-1}, g_m)$ with $t \geq m$ denote the counterfactual outcome that would be observed had the patient received their observed treatments \bar{A}_{m-1} through time $m-1$ then followed strategy g from time m onward. Here, the treatment strategy g is typically specified by the domain experts, e.g. clinicians. In this work, the outcome Y_t can be deemed to be a variable in the vector L_{t+1} .

In counterfactual point prediction, our goal is to estimate expected counterfactual patient outcome trajectories

$$\{E[Y_t(\bar{A}_{m-1}, \underline{g}_m)|H_m], t \geq m\} \quad (1)$$

given observed patient history through time m for any m and any specified treatment strategy g , where g is specified by a domain expert, e.g. a clinician. It may be of interest to estimate the counterfactual outcome distributions at future time points

$$\{p(Y_t(\bar{A}_{m-1}, \underline{g}_m)|H_m), t \geq m\}. \quad (2)$$

The g-computation algorithm enables the estimation of (1) and (2) under the following assumptions (Robins, 1986): Consistency, Sequential Exchangeability, and Positivity.

Assumption 3.1. Consistency asserts that the observed outcome aligns with the counterfactual outcome that would have occurred had the observed treatment been applied.

Assumption 3.2. Sequential exchangeability requires that there is no unobserved confounding, i.e., all drivers of treatment decisions prognostic for the outcome are included in the data.

Assumption 3.3. Positivity posits that the counterfactual treatment strategy of interest has some non-zero probability of actually being implemented.

Under assumptions 3.1-3.3, for $t = m$ we have that

$$p(Y_m(\bar{A}_{m-1}, \underline{g}_m)|H_m) = p(Y_m|H_m, A_m = g_m(H_m)), \quad (3)$$

i.e. the conditional distribution of the counterfactual is the conditional distribution of the observed outcome given patient history and given that treatment follows the strategy of interest. For $t > m$, we need to adjust for time-varying confounding. With $X_{i:j} = X_i, \dots, X_j$ for any random variable X , under assumptions 1-3 the g-formula yields

$$\begin{aligned} p(Y_t(\bar{A}_{m-1}, \underline{g}_m) = y|H_m) \\ = \int_{l_{m+1:t}} p(Y_t = y|H_m, L_{m+1:t} = l_{m+1:t}, A_{m:t} = g(H_{m:t})) \\ \times \prod_{j=m+1}^t p(L_j = l_j|H_m, L_{m+1:j-1} = l_{m+1:j-1}, \\ A_{m,j-1} = g(H_m, l_{m+1:j-1})). \end{aligned} \quad (4)$$

We can approximate this integral through Monte-Carlo simulation.

G-computation algorithm requires the ability to simulate from joint conditional distributions $p(L_t|\bar{L}_{t-1}, \bar{A}_{t-1})$ of the covariates given patient history at time t . These conditional distributions need to be estimated from data. Most implementations of g-computation use generalized linear regression models (GLMs) to estimate the conditional distributions of the covariates. These models often do not capture the complex temporal dependencies in the patient data. We propose the G-Transformer for this task.

3.2. G-Transformer Architecture

We utilized two Transformer encoders as the sequential model to separately learn hidden representations for continuous and categorical covariates in G-Transformer. We use the

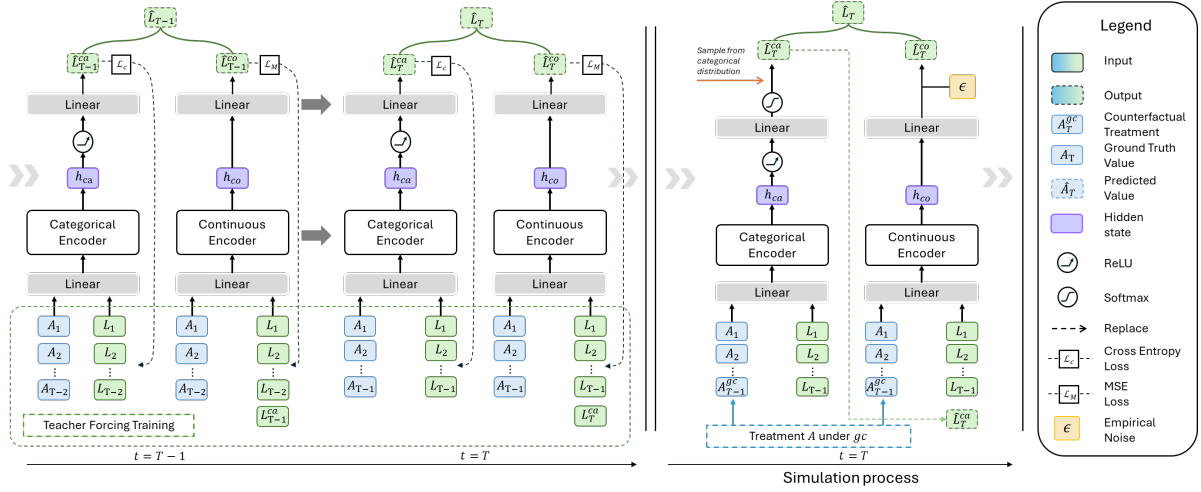


Figure 1: G-Transformer Architecture. G-Transformer uses two distinct encoders for categorical (L^{ca}) and continuous variables (L^{co}) respectively. The diagram illustrates (i) the training process through time steps $T-1$ and T , and (ii) the counterfactual simulation process starting at time T , with the counterfactual strategy initiated at the end of time $T-1$. Teacher forcing is used during training.

teacher forcing in the training process and g-computation at simulation process. The architecture is shown in Fig.1.

Let L_t^0, \dots, L_t^p denote p components of the vector of covariates L_t . When we calculate joint conditional distributions $p(L_t | \bar{L}_{t-1}, \bar{A}_{t-1})$ at time t , we leverage the conditional probability identity as in (Li et al., 2021):

$$\begin{aligned} p(L_t | \bar{L}_{t-1}, \bar{A}_{t-1}) &= p(L_t^0 | \bar{L}_{t-1}, \bar{A}_{t-1}) \\ &\times p(L_t^1 | L_t^0, \bar{L}_{t-1}, \bar{A}_{t-1}) \\ &\times \dots \\ &\times p(L_t^{P-1} | L_t^0, \dots, L_t^{P-2}, \bar{L}_{t-1}, \bar{A}_{t-1}) \end{aligned} \quad (5)$$

In G-Transformer, we divide covariates into two groups: one for categorical variables L_t^{ca} , and the other for continuous variables L_t^{co} . Thus, $p(L_t | \bar{L}_{t-1}, \bar{A}_{t-1})$ is defined as:

$$p(L_t | \bar{L}_{t-1}, \bar{A}_{t-1}) = p(L_t^{ca} | \bar{L}_{t-1}, \bar{A}_{t-1}) \times p(L_t^{co} | L_t^{ca}, \bar{L}_{t-1}, \bar{A}_{t-1}) \quad (6)$$

Although assigning a customized model to each covariate may achieve better performance, considering the limitations of computational resources and the potential dependencies among variables, we decide to have only two Transformer encoder models to perform representation learning for categorical variables and continuous variables, respectively. At each time step t , we can compute representation of patient history $R_t = r_t(\bar{L}_t, \bar{A}_t; \theta)$, where θ denotes the learnable parameters from model r_t . We will introduce the specific content of model r_t in the following section.

Representation Learning. For the input of categorical encoder, we concatenate all the historical treatments \bar{A}_t and covariates \bar{L}_t together, and use a linear layer to obtain their combined representation h_{ca}^r :

$$h_{ca}^r = \text{Linear}(\text{concat}(\bar{A}_t, \bar{L}_t)) \quad (7)$$

Afterwards, we feed the combined representations of treatments and outcomes h_{ca}^e into a Transformer encoder to obtain the final representation of past covariate history:

$$h_{ca} = \text{Transformer Encoder}_{ca}(h_{ca}^r) \quad (8)$$

The internal architecture of the Transformer encoder sublayers follows the original Transformer paper (Vaswani et al., 2017), including a multi-head self-attention layer, feed-forward network, and layer normalization mechanism. After obtaining h_{ca} , we map the hidden representation to the predicted future time step through a linear layer:

$$\bar{L}_{t+1}^{ca} = \text{Linear}(\text{ReLU}(h_{ca})) \quad (9)$$

During the training phase, we use **teacher forcing** to guide the training of the categorical and continuous encoders. In addition to the patient’s historical sequences (\bar{A}_t, \bar{L}_t) , we also use observed value L_{t+1}^{ca} as input into the continuous encoder:

$$h_{co}^r = \text{Linear}(\text{concat}(\bar{A}_t, \bar{L}_t, L_{t+1}^{ca})). \quad (10)$$

As with categorical variables, we use a Transformer encoder to obtain a hidden representation h_{co} that incorporates the guiding variables. Then we utilize a linear layer to modify the hidden state to final output \bar{L}_{t+1}^{co} :

$$h_{co} = \text{Transformer Encoder}_{co}(h_{co}^r) \quad (11)$$

$$\bar{L}_{t+1}^{co} = \text{Linear}(h_{co}) \quad (12)$$

3.3. Training of G-Transformer

Since G-computation attempts to model the joint conditional probability distribution of the next time step $p(L_t | \bar{L}_{t-1}, \bar{A}_{t-1})$ given the observable sequence, this approach is more aligned with the modeling methods of some RNN-like linear regression models. However, due to the Transformer’s nature as a seq-2-seq model, its multi-head self-attention mechanism endows it with powerful parallel computing capabilities. Therefore, the Transformer encoder is more inclined to model the probability distribution of a sequence, that is $p(\bar{L}_{2:t} | \bar{L}_{1:t-1}, \bar{A}_{1:t-1})$. We tried two different training methods on our counterfactual prediction task, and the results are shown in the Appendix A.1. Furthermore, in real-world scenarios, most treatment variables appear in binary form, with few treatment variables presented in continuous form. Therefore, we believe that prioritizing modeling for categorical variables can provide more insights for the prediction of continuous variables. This approach also aligns more closely with the fundamental procedural form we use in the simulation process to calculate treatment variable $a_m = g_m(H_m)$ in Algorithm. 2. After completing the entire prediction process, we use cross-entropy loss and MSE (Mean Squared Error) loss to optimize

the prediction results for categorical and continuous variables, respectively. For categorical variables:

$$\mathcal{L}_{ce} = -\frac{1}{N \times P_{ca}} \sum_i^N \sum_{c=1}^{P_{ca}} y_{ic} \log(p_{ic}; \theta) \quad (13)$$

where P_{ca} denotes the number of categorical variables, N denotes the number of patients, and θ denotes the model parameters. In fact, we separately calculated the cross-entropy losses of different variables and computed their averages to account for the needs of multi-class variables. For continuous variables, we utilize the MSE loss:

$$\mathcal{L}_{mse} = \frac{1}{N} \sum_{i=1}^N \sum_{t=1}^K \|\bar{L}_{t,i}^{co} - \hat{L}_{t,i}^{co}\|^2 \quad (14)$$

where $\hat{L}_{t,i}^{co}$ denotes the output of continuous encoder part of G-Transformer for patient i in time t , N denotes number of patients and K denotes length of time. Algorithm 1 illustrates the overall training process of G-Transformer.

Algorithm 1: G-Transformer training algorithm

Input: Training set \mathcal{D} data tuples: $\mathcal{D} = \{(\bar{L}, \bar{A})\}$; the number of the prediction length l , Model parameters θ_{ca} and θ_{co} ; the number of the learning epochs E .

while $e < E$ **do**

- for** $t = 2$ **to** l **do**
 - Concatenate treatment variables and outcome variables $\bar{Y}_{1:t-1} = \{\bar{L}_{1:t-1}, \bar{A}_{1:t-1}\}$.
 - Use categorical encoder to compute the $\bar{Y}_{2:t}^{ca} = f_{ca}(\bar{Y}_{1:t-1}; \theta_{ca})$.
 - Keep the last time step of the predicted categorical variable $\bar{Y}_t^{ca} = \{\bar{L}_t^{ca}, A_t^{ca}\}$.
 - Use **teacher forcing** to process the input of continuous encoder $\bar{Y}_{1:t-1}^{te} = \{\bar{L}_{1:t-1}, \bar{A}_{1:t-1}, \bar{L}_t^{ca}\}$.
 - Use continuous encoder to compute the $\bar{Y}_{2:t}^{co} = f_{co}(\bar{Y}_{1:t-1}^{te}; \theta_{co})$.
 - Keep the last time step of the predicted continuous variable $\bar{Y}_t^{co} = \{\bar{L}_t^{co}, A_t^{co}\}$.
 - Save the last time step Y_t^{co}, Y_t^{ca} .
- end**
- Concatenate the results of all predicted time steps $\bar{Y}_{2:t}^{ca} = \{Y_2^{ca}, \dots, Y_t^{ca}\}$ and $\bar{Y}_{2:t}^{co} = \{Y_2^{co}, \dots, Y_t^{co}\}$.
- Update model parameters θ_{ca} and θ_{co} by minimizing (13) and (14) with gradient descent

end

return *updated model parameters θ_{ca} and θ_{co}*

3.4. Simulation

After having a trained sequential model $f(R; \theta)$, we can obtain the conditional expectation estimate $\mathbb{E}[L_t | \bar{L}_{t-1}, \{L_t^i\}_{i=1, \dots, p}, \bar{A}_{t-1}]$ of all p covariates at time step t through Monte Carlo simulation. Without making parametric assumptions, we could simulate from:

$$L_t^p \simeq \hat{\mathbb{E}}[(L_t^p | L_t^0, \dots, L_t^{p-1}, \bar{L}_{t-1}, \bar{A}_{t-1})] + \epsilon_t^p \quad (15)$$

where ϵ_t^p is a noise which draws from the empirical distribution of the residuals $L_t^p - \hat{L}_t^p$ in a holdout set. If the variable is binary, then ϵ_t^p here is sampled from a Bernoulli distribution parameterized by empirical data. Afterward, we use Algorithm 2 for K times to perform multi-timestep simulations. Figure 1 illustrates the simulation process. Different from the training process, since we cannot access to the ground truth, we sample from the learned conditional distribution when performing counterfactual predictions. For categorical variables, we use the parameters derived from the result \hat{L}^{ca} of the categorical encoder to parameterize a categorical distribution (or a Bernoulli for binary indicator variables), and sample from the corresponding distribution. For the continuous variables, we added noise sampled from the empirical distribution collected from the validation set to the output part of the continuous encoder.

Algorithm 2: Simulation (one time-step)

Set $a_m^* = g_m(H_m)$
 Sample l_{m+1}^* from $p(L_{m+1}|H_m, A_m = a_m^*)$
 Set $a_{m+1}^* = g_m(H_m, l_{m+1}^*, a_m^*)$
 Sample l_{m+2}^* from $p(L_{m+2}|H_m, L_{m+1} = l_{m+1}^*, A_m = a_m^*, A_{m+1} = a_{m+1}^*)$
 Continue simulations through time K

We repeat the g-computation simulation Algorithm M times. At the end of this process, we have M simulated draws of the counterfactual outcome for each time $t = \{m, \dots, K\}$. For each t , the empirical distribution of these draws constitutes a Monte-Carlo approximation of the counterfactual outcome distribution (2). The sample averages of the draws at each time t are an estimate of the conditional expectations (1) and can serve as point predictions for $Y_t(\bar{A}_{m-1}, \underline{g}_m)$ in a patient with history H_m .

3.5. Evaluation

To evaluate G-Transformer, we use simulated data in which counterfactual ground truth can be known. Specifically, we use CVSim (Heldt et al., 2010), a well-established mechanistic model of the cardiovascular system, to simulate counterfactual patient trajectories under various dynamic fluid and vasopressor administration strategies. Additionally, using a simulated tumor growth data set, we compare G-Transformer with recently introduced G-Net (Li et al., 2021), Recurrent Neural Networks (CRN) (Bica et al., 2020a), a Recurrent Marginal Structural Network (R-MSN) (Lim et al., 2018), a recurrent neural network implementation of a history adjusted marginal structural model for estimating static time-varying treatment effects, and Causal Transformer (Melnychuk et al., 2022).

We applied our proposed G-Transformer approach to predicting outcomes of sepsis patients in the ICU under alternative fluid resuscitation treatment regimes (e.g. aggressive vs. conservative) using de-identified real-world intensive care units (ICU) data from the MIMIC-IV (Johnson et al., 2023b) publicly available from PhysioNet.

We quantitatively evaluate G-Transformer’s performance in predicting patient trajectories under observational treatment regimes learned from the ICU data. This entails using the G-Transformer architecture to predict treatment at each time-step under the “usual care”

in the observational data. Under predictive check, the treatments are from G-Transformer predicted actions conditioned on patient history.

4. Experiments on Simulated Data from Mechanistic Models

4.1. Cancer Growth Experiments and Results

Cancer Growth Data Generation As in [Lim et al. \(2018\)](#); [Bica et al. \(2020a\)](#); [Li et al. \(2021\)](#); [Melnychuk et al. \(2022\)](#), we generate simulated ‘observational’ data from a pharmacokinetic-pharmacodynamic model of tumor growth under a stochastic regime ([Geng et al., 2017](#)). In this simulation, chemotherapy and radiation therapy comprise a two dimensional time-varying treatment impacting tumor growth. Under the observational regime, probability of receiving each treatment at each time depends on volume history, so there is time-varying confounding. We use the same experiment settings and data generation procedure as reported in [Li et al. \(2021\)](#). We generated four test sets in which four counterfactual regimes were followed for the final four time points in the test set: (1) give only radiotherapy, (2) only chemotherapy, (3) both chemotherapy and radiotherapy, and (4) no treatment. These counterfactual regimes are static time-varying regimes (in which treatments do not depend on prior patient history), as rMSN, CRN, and Causal Transformer are intended to estimate counterfactuals under static time-varying regimes.

Table 1 presents the percent root mean square error (RMSE) of predictions from rMSN, CRN, linear implementation of g-computation, G-Net, Causal Transformer, and G-Transformer in the final four time steps when counterfactual strategies were in effect, conditioned upon previous time points. The raw RMSE values were divided by the maximum possible tumor volume, 1150 cm^2 , as in [Lim et al. \(2018\)](#), to calculate the percent RMSE.

We observe that G-Transformer achieved the best overall RMSE performance in three of the four cancer growth datasets, demonstrating its advantages in counterfactual prediction task compared to other state-of-the-art deep learning models, including rMSN, CRN, G-Net and Causal Transformer. Causal Transformer outperformed other models under the chemotherapy (Chemo) counterfactual regime, but fall short in all other counterfactual regimes.

4.2. CVSim Experiments and Results

CVSim Data Generation To evaluate counterfactual predictions, it is necessary to use simulated data in which counterfactual ground truth for outcomes under alternative treatment strategies is known. To this end, we performed experiments on data generated by CVSim, a program that simulates the dynamics of the human cardiovascular system ([Heldt et al., 2010](#)). We used a CVSim 6-compartment circulatory model which takes as input 28 variables that together govern a hemodynamic system. We built on CVSim by adding stochastic components and interventions for the purposes of evaluating our counterfactual simulators.

We generated an ‘observational’ dataset D_o under treatment regime g_o and two ‘counterfactual’ datasets D_{c1} and D_{c2} under treatment regimes g_{c1} and g_{c2} . The data generating processes producing D_o and D_{cj} were the same except for the treatment assignment rules.

Table 1: Cancer growth data: Percent RMSE for various prediction horizons. A = Overall. CT = Causal Transformer. Best performing models in bold.

| | | t | rMSN | CRN | Linear | G-Net | CT | Ours |
|-------------|---|------|------|------|-------------|-------------|-------------|---------------|
| | | | - | - | g-comp | - | - | G-Transformer |
| No Treat | 1 | 1.13 | 1.00 | 0.63 | 0.25 | 0.67 | 0.26 | |
| | 2 | 1.24 | 1.20 | 1.21 | 0.47 | 0.65 | 0.44 | |
| | 3 | 1.85 | 1.49 | 1.78 | 0.72 | 0.63 | 0.55 | |
| | 4 | 2.60 | 1.78 | 2.35 | 1.01 | 0.63 | 0.66 | |
| | A | 1.68 | 1.40 | 1.62 | 0.67 | 0.65 | 0.48 | |
| Radio | 1 | 5.27 | 4.91 | 7.14 | 3.29 | 5.15 | 2.74 | |
| | 2 | 5.38 | 4.92 | 7.43 | 3.14 | 2.98 | 2.50 | |
| | 3 | 5.13 | 4.94 | 7.05 | 3.02 | 2.72 | 2.40 | |
| | 4 | 4.81 | 4.92 | 6.50 | 3.00 | 2.53 | 2.52 | |
| | A | 5.15 | 4.92 | 7.04 | 3.11 | 3.35 | 2.54 | |
| Chemo | 1 | 1.42 | 1.04 | 1.58 | 0.34 | 0.66 | 0.36 | |
| | 2 | 1.27 | 1.09 | 3.14 | 0.63 | 0.50 | 1.16 | |
| | 3 | 1.46 | 1.03 | 4.52 | 0.84 | 0.44 | 1.95 | |
| | 4 | 1.69 | 1.02 | 5.47 | 0.89 | 0.41 | 2.45 | |
| | A | 1.47 | 1.05 | 3.96 | 0.71 | 0.50 | 1.48 | |
| Radio Chemo | 1 | 4.76 | 4.66 | 7.76 | 3.10 | 8.40 | 2.48 | |
| | 2 | 3.59 | 4.36 | 7.32 | 2.28 | 7.72 | 2.04 | |
| | 3 | 2.76 | 3.65 | 6.13 | 1.50 | 7.79 | 1.54 | |
| | 4 | 2.30 | 2.95 | 4.88 | 1.18 | 7.67 | 1.10 | |
| | A | 3.48 | 3.96 | 6.62 | 2.15 | 7.90 | 1.79 | |

For each j , g_{cj} was identical to g_o for the first $m - 1$ simulation time steps before diverging to a different treatment rule for time steps m to K . Full details are in the Appendix C.

Experiment As in Li et al. (2021), we generated a total of 12,000 trajectories in D_o ($N_o = 12,000$), of which 80% were used for training, and the remaining 20% for validation. For testing, we generated 1000 observations in the D_{cj} datasets ($N_c = 1000$). We included a total of 20 output variables (i.e. two treatment variables and 18 covariates influencing treatment assignment under g_o) from CVSIm to construct D_o and D_{cj} ; each trajectory is of length 66 time steps (d=20, K=66). In each D_{cj} , the switching time point m from g_o to g_c is fixed at 34 for all trajectories ($m = 34$).

Given observed covariate history through 34 time steps and treatment history through 33 time steps of each trajectory in each D_{cj} , we computed both the population-level and individual-level RMSE, as well as the calibration, of counterfactual predictions from G-Transformer and its counterparts for time steps 35 to 66. Moreover, we presented the estimated and actual population-level average trajectories under g_{c1} and g_{c2} for selected variables. We also visually demonstrated the treatment effects estimation.

Population-Level and Individual-Level RMSE We use both population-level and individual-level RMSE to assess the predictive accuracy of the model for continuous vari-

ables in CVSim data. To derive population-level RMSE, we aggregated the simulated trajectories from all patients into a single population-level trajectory. This predicted average population-level trajectory was then compared to the ground-truth average population-level trajectory for RMSE calculation. Individual-level RMSE is calculated by first determining the square root of the mean squared differences between each patient’s observed and predicted trajectories. For G-Transformer, G-Net and the linear implementation of g-computation, the predicted trajectory is averaged from 100 Monte Carlo simulations conditioned on historical data up to time ($k-1$). The RMSE values across all patients are then averaged to derive individual-level RMSE.

Table 2 presents a comparison of individual-level and population-level RMSE among linear implementation of g-computation, G-Net, Causal Transformer, and G-Transformer under g_{c1} and g_{c2} . The G-Transformer outperforms linear implementation of g-computation and G-Net, and considerably outperforms Causal Transformer in this counterfactual prediction task. It should be noted that Causal Transformer [Melnychuk et al. \(2022\)](#) can estimate counterfactual outcomes under time-varying treatments, but it is not designed to estimate counterfactual outcomes under *dynamic* treatment regimes, where treatments depend on past covariate history. Nevertheless, we present its performance here as a baseline.

Table 2: CVSim: Counterfactual prediction under g_{c1} and g_{c2} . Performance of various models in predicting remaining 32-hour patient covariate trajectories based on first 34-hour patient covariate trajectories. Values reported represent the population-level and individual-level RMSE between the predicted and counterfactual trajectories.

| Model | Population Level | | Individual Level | |
|--------------------|------------------------|------------------------|------------------------|------------------------|
| | $\text{RMSE}_{g_{c1}}$ | $\text{RMSE}_{g_{c2}}$ | $\text{RMSE}_{g_{c1}}$ | $\text{RMSE}_{g_{c2}}$ |
| Linear(g-comp) | 0.252 | 0.272 | 1.103 | 1.193 |
| G-Net | 0.061 | 0.105 | 1.020 | 1.114 |
| Causal Transformer | 0.885 | 1.099 | 1.435 | 1.727 |
| G-Transformer | 0.050 | 0.054 | 1.016 | 1.104 |

Calibration We assess the calibration of a G-Transformer, G-Net, or linear implementation of g-computation, denoted as G , as follows. Given lower and upper quantiles α_{low} and α_{high} , the calibration measures the frequency with which the actual counterfactual covariate $L_{ti}^{h,cj}$ is between the α_{low} and α_{high} quantiles of the M simulations $\{\tilde{L}_{ti}^{h,cj}(H_{mi}^{cj}, G, k) : k \in 1 : M\}$. If this frequency is approximately $\alpha_{high} - \alpha_{low}$, then G is well calibrated.

Figure 2 depicts calibration for G-Transformer, G-Net, and linear implementation of g-computation with lower and upper quantiles of 0.05 and 0.95. G-Transformer generally performed better than G-Net and linear implementation of g-computation over all time steps. The model is well calibrated at the beginning, but as simulation time steps increases, calibration becomes weaker for all models. This is in line with the RMSE increase over time as can be seen from Table 7 in the Appendix A.3.

Population-Level Trajectories The G-Transformer, G-Net, and linear implementation of g-computation can be used to quantitatively demonstrate counterfactual outcomes through population average trajectories. The estimated and actual population-level average

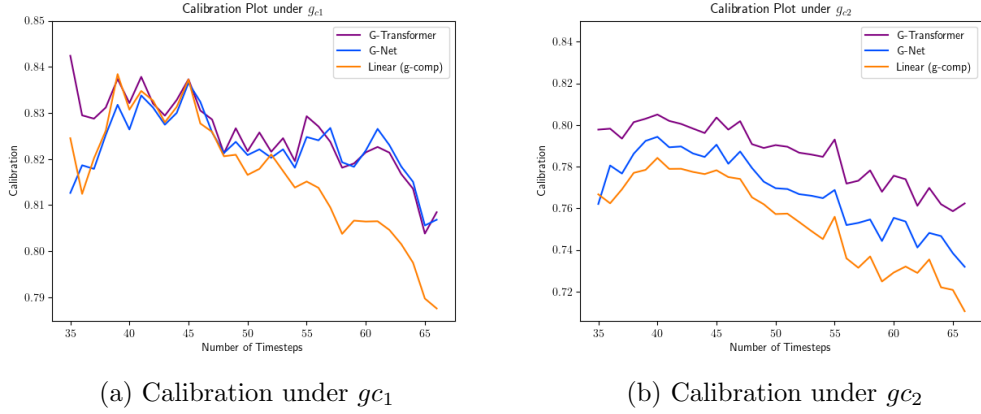


Figure 2: Calibration over time for g_{c1} and g_{c2}

trajectories under g_{c1} and g_{c2} for selected variables, specifically arterial flow (AQ), arterial pressure (AP), and heart rate (HR), are presented in Figure 3 (a) to (f). The plots show that G-Transformer outperforms G-Net and linear g-computation implementation, and more accurately predict AQ, AP, and HR counterfactual trajectories from the population level.

Treatment Effects The G-Transformer, G-Net, and linear g-computation implementation can also be used to estimate population average counterfactual outcomes and treatment effects, quantities sometimes more relevant to policy decisions than individual-level counterfactual predictions. Figure 3 (g) to (i) show the estimates and true values of the population average treatment effect of following g_{c1} as opposed to g_{c2} on selected variables. We see that the G-Transformer effectively estimates these population-level quantities of interest.

5. Experiments on MIMIC Data

5.1. MIMIC Cohort

The data employed in this study was extracted from the Medical Information Mart for Intensive Care IV database (MIMIC-IV v1.0), containing medical records from more than 523,500 hospital admissions and 76,500 ICU stays at the Beth Israel Deaconess Medical Center (BIDMC) between 2008 and 2019 [Johnson et al. \(2023a\)](#). Our cohort consists of ICU patient identified as septic under the Third International Consensus Definitions for Sepsis and Septic Shock (Sepsis-3) [Singer et al. \(2016\)](#) and did not meet exclusion criteria (see Appendix D for details). Our final sepsis cohort consisted of 8,934 total patients which we further split into 7,147 patients, 893 patients, and 894 patients for the training, validation, and test data respectively.

5.2. Study Design

Since there is no ground-truth observations available for the MIMIC data for counterfactual predictions, we first assess our models’ performance through a “predictive check.” This

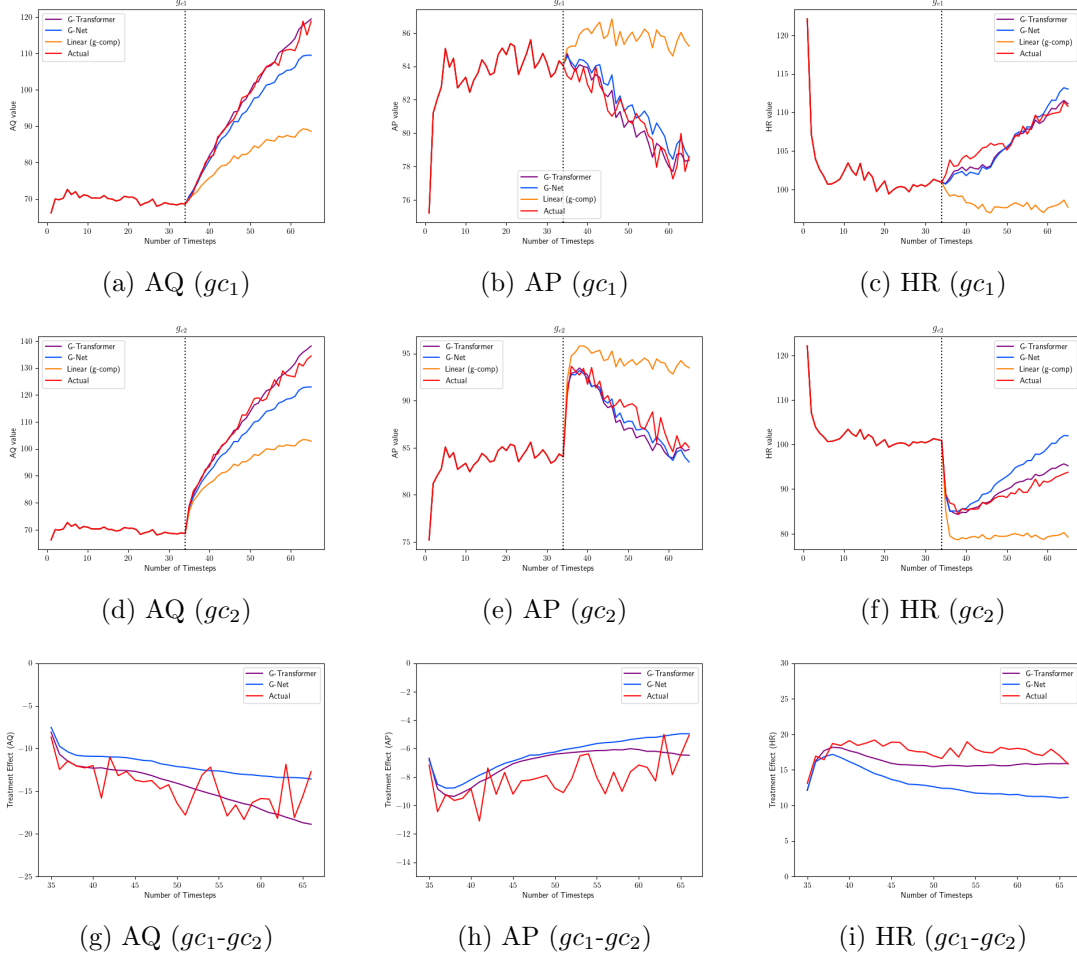


Figure 3: Plots (a) to (f) show the estimated and actual population average trajectories for three selected variables: arterial flow (AQ), arterial pressure (AP), and heart rate (HR), according to three models’ predictions under g_{c1} vs g_{c2} . Plots (g) to (i) show population-level treatment effect of g_{c1} vs g_{c2} estimated by G-Transformer vs G-Net.

involved conducting Monte Carlo simulations and projecting forward patient covariate trajectories within the test set under the observational regime. Subsequently, we compared these simulated trajectories (averaged across 100 Monte Carlo simulations per patient) to the ground-truth data. Following predictive check, we assess our model in performing counterfactual predictions.

Predictive Checks We compared the 24-hour trajectories between predicted and ground-truth under G-Transformer, G-Net, and Causal Transformer, using individual-level and population-level RMSE as metrics. The method for calculating the population-level RMSE is as described in the previous section. However, since patient trajectories can be censored due to events such as death and release in MIMIC data, individual-level RMSE is adjusted

to account for error due to over- and under-prediction in the trajectory length as in [Su et al.](#) (see Appendix B.1 for details).

We also compared the models' performance in predicting the occurrence of adverse clinical outcomes during the first 24-hours patients were in the ICU. Confidence intervals around AUCs are generated based on techniques described in [DeLong et al. \(1988\)](#). To generate a probability for the 24-hour window, we first assigned a binary label for each Monte Carlo simulation based on whether the outcome is predicted to have occurred: 1 if outcome of interest was predicted to occur between timestamps k to 24, and 0 otherwise. Then the average across the Monte Carlo simulations per patient was used as the predicted probability for that patient. The ground truth was determined in the same manner by looking for the presence of the outcome of interest in the ground-truth trajectory.

Counterfactual Experiments We adapted our counterfactual strategies from established clinical trials studying the early treatment of sepsis. This strategy imposes a fluid cap on the total amount of fluids intake of a patient to X liters, and ceases administration once the fluid cap is reached or when the patient is fluid-overloaded. More specifically, this strategy was based on the Crystalloid Liberal or Vasopressors Early Resuscitation in Sepsis (CLOVERS) clinical trial ([Self et al.](#)). For a patient with blood pressure below 65mmHg at time t , a 1000mL bolus was administered if the total volume of fluids (including both treatment and maintenance) they received up until that time point did not exceed X liters and if they did not exhibit any signs of fluid overload (as indicated by the presence of pulmonary edema based on chest x-ray radiology reports). We experimented with imposing a fluid cap of 3L and 5L as fluid conservative strategies, and a fluid strategy with no fluid cap to represent a fluid liberal strategy.

5.3. Predictive Check: Population-Level and Individual-Level RMSE

Table 3 presents the predictive check on population-level and individual-level RMSE for continuous variables. We aim to assess the performance of G-Transformer, G-Net, and Causal Transformer in predicting 24-hour patient covariate trajectories, starting at time k conditioned on covariates from the previous $k-1$ timesteps of post-ICU admission. k ranges from 2 to 8 hours after ICU admission. Values reported represent the RMSE of continuous covariates between the predicted and ground-truth trajectories. To account for mismatch in trajectory length due to over- and under-prediction of death and release time, for both predicted and actual trajectories, depending on nature of covariates, post-death timesteps are padded with one of the following values: normalized zero, normalized minimum value in dataset, or normalized logarithmic zero. The post-release timesteps are consistently padded with normalized population mean.

According to Table 3, we can see that errors in predicted 24-hour patient trajectories are relatively stable for G-Transformer and Causal Transformer, and G-Transformer consistently outperforms G-Net and Causal Transformer across different values of k . Although Causal Transformer [Melnichuk et al. \(2022\)](#) is not intended to estimate counterfactual outcomes under **dynamic** treatment regimes (where treatments depend on past covariate history), nevertheless, we present its performance here as a baseline.

Predictive Check: an Illustrative Example from G-Transformer's Monte Carlo Simulations Figure 4 illustrates the Monte Carlo simulations generated by G-Transformer

Table 3: MIMIC-IV Experiments: Predictive check on continuous variables at population-level and individual-level RMSE. k is the simulation start time relative to the ICU admission time. Performance in predicting 24-hour patient covariate trajectories, starting at hour k conditioned on covariates from the previous $k - 1$ timesteps of post-ICU admission. k ranges from 2 to 8 hours after ICU admission. Values reported represent the population-level and individual-level RMSE of continuous covariates between the predicted and ground-truth trajectories. Individual-level RMSE is adjusted to account for error due to over- and under-prediction in the trajectory length as a result of death and discharge.

| Model / k (hours) | Population Level RMSE | | | | Individual Level RMSE | | | |
|----------------------|-----------------------|--------------|--------------|--------------|-----------------------|-------------|-------------|-------------|
| | 2 | 4 | 6 | 8 | 2 | 4 | 6 | 8 |
| G-Net | 0.338 | 0.265 | 0.214 | 0.181 | 15.85 | 13.71 | 11.40 | 9.29 |
| Causal Transformer | 2.770 | 2.736 | 2.643 | 2.514 | 14.37 | 15.00 | 15.73 | 16.54 |
| G-Transformer | 0.297 | 0.233 | 0.204 | 0.178 | 7.96 | 8.83 | 9.46 | 8.62 |

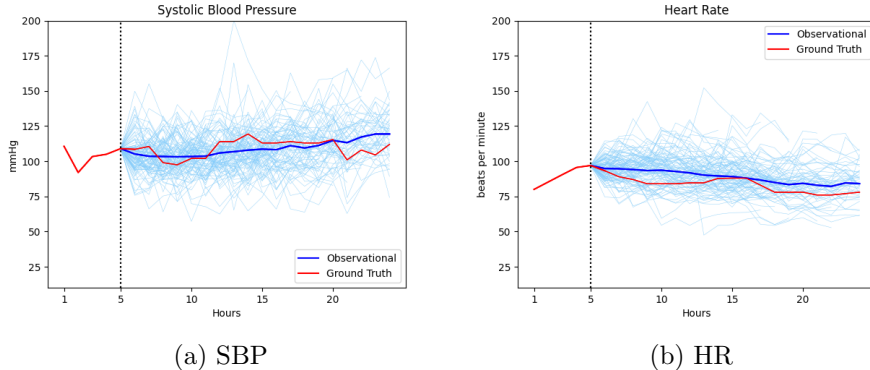


Figure 4: Illustration of predictive check on an example MIMIC test set patient. G-Transformer simulated systolic blood pressure (SBP) and heart rate (HR) trajectories (100 Monte Carlo simulations in light blue, average in solid dark blue) compared with ground truth (red) for one patient under predictive check (simulation starting at hour 6).

for selected variables, specifically systolic blood pressure (SBP) and heart rate (HR), given an example MIMIC patient from test dataset. We observe that the predicted trajectory averaged from 100 Monte Carlo simulations follow closely with the ground-truth trajectory.

Predictive Check: 24-Hour Outcomes Predictions Table 4 presents AUCs (and 95% CI) in predicting clinical outcomes within the first 24 hours of ICU admission at varying simulation start times from G-Transformer and G-Net. There are six outcomes of interest: diagnosis of pulmonary edema, use of a mechanical ventilator (MV), administration of diuretics, dialysis, ICU release, and in-hospital mortality. We observe that the predicted 24-hour clinical outcomes of interest tend to be more accurate as the value of k increases, and G-Transformer generally outperforms G-Net across different values of k .

Counterfactual Prediction: Population-Level Trajectories We used G-Transformer to simulate covariate trajectories for patients in the test dataset under two conservative flu-

ids strategies (with 3L and 5L fluid cap) and a fluid liberal strategy (with no cap). Selected covariates are presented in Figure 5, allowing for comparison of the three counterfactual regimes. Population-level average trajectories were calculated from the test set (N=894). Counterfactual strategies are applied starting at time step 1, conditioned on observations up until the first hour in the ICU. For each patient, we perform 100 Monte Carlo simulations. The plotted values are averaged across simulated trajectories for all test patients.

Our aim is to assess whether G-Transformer can make logical and clinically meaningful counterfactual predictions. The trends depicted in Figure 5 align with our physiological expectations. Under fluid liberal strategies, the bolus volume, urine output, respiratory rate, and blood pressure exhibit higher values, following the expected trends at a population level. Conversely, the higher levels in creatinine and blood urea nitrogen (BUN) noted under the fluids conservative regime also align with expected outcomes.

Readers should exercise caution when interpreting these plots in Figure 5 as indicators of treatment effects, as the number of patients (or trajectories) contributing to the average may not remain constant throughout the entire 24-hour period. Simulated trajectories might terminate prematurely within the 24-hour period due to death or discharge.

6. Discussion and Conclusion

In this paper, we present G-Transformer, a Transformer-based framework supporting g-computation, to estimate clinical outcomes under counterfactual treatment strategies from both synthetic dataset and a real-world sepsis patient cohort. Our experiments using Cancer Growth and CVSim data, demonstrated that G-Transformer achieved superior performance over other state-of-the art approaches. Using a real-world sepsis dataset, we demonstrated that G-Transformer provides clinically meaningful forecasts of covariate trajectories under alternative counterfactual fluid limiting regimes. This study highlights G-Transformer’s potential clinical utility in supporting treatment decisions for ICU patients. Although we focus on applications in healthcare in this study, the G-Transformer architecture can be applied to other sequential decision making tasks that involve dynamic and time-varying interventions.

Table 4: Predictive Check. Performance of G-Transformer and G-Net in predicting clinical outcomes within the first 24 hours of ICU admission at varying simulation start times. Values reported are AUCs and 95% confidence intervals.

| Model | k | Edema | MV | Diuretics | Dialysis | Release | Death |
|----------------------|----------|--------------------------|--------------------------|--------------------------|--------------------------|--------------------------|--------------------------|
| G-Net | 2 | 0.82 (0.79, 0.86) | 0.89 (0.87, 0.91) | 0.68 (0.63, 0.73) | 0.85 (0.75, 0.95) | 0.67 (0.61, 0.73) | 0.79 (0.67, 0.90) |
| G-Transformer | 2 | 0.84 (0.80, 0.87) | 0.89 (0.86, 0.91) | 0.73 (0.68, 0.78) | 0.90 (0.81, 0.98) | 0.67 (0.61, 0.73) | 0.82 (0.71, 0.93) |
| G-Net | 4 | 0.86 (0.83, 0.89) | 0.94 (0.92, 0.95) | 0.70 (0.64, 0.75) | 0.94 (0.88, 1.00) | 0.65 (0.59, 0.71) | 0.86 (0.76, 0.96) |
| G-Transformer | 4 | 0.86 (0.83, 0.89) | 0.94 (0.92, 0.96) | 0.75 (0.70, 0.80) | 0.96 (0.91, 1.00) | 0.68 (0.62, 0.74) | 0.91 (0.83, 1.00) |
| G-Net | 6 | 0.89 (0.86, 0.92) | 0.95 (0.93, 0.96) | 0.73 (0.67, 0.78) | 0.93 (0.86, 1.00) | 0.68 (0.63, 0.74) | 0.83 (0.72, 0.94) |
| G-Transformer | 6 | 0.87 (0.84, 0.90) | 0.94 (0.92, 0.96) | 0.74 (0.69, 0.80) | 0.96 (0.90, 1.00) | 0.69 (0.63, 0.74) | 0.89 (0.80, 0.98) |
| G-Net | 8 | 0.89 (0.87, 0.92) | 0.95 (0.94, 0.97) | 0.73 (0.68, 0.79) | 0.97 (0.92, 1.00) | 0.71 (0.66, 0.77) | 0.89 (0.79, 0.98) |
| G-Transformer | 8 | 0.89 (0.86, 0.91) | 0.95 (0.93, 0.97) | 0.75 (0.70, 0.81) | 0.95 (0.89, 1.00) | 0.71 (0.66, 0.77) | 0.95 (0.79, 0.98) |

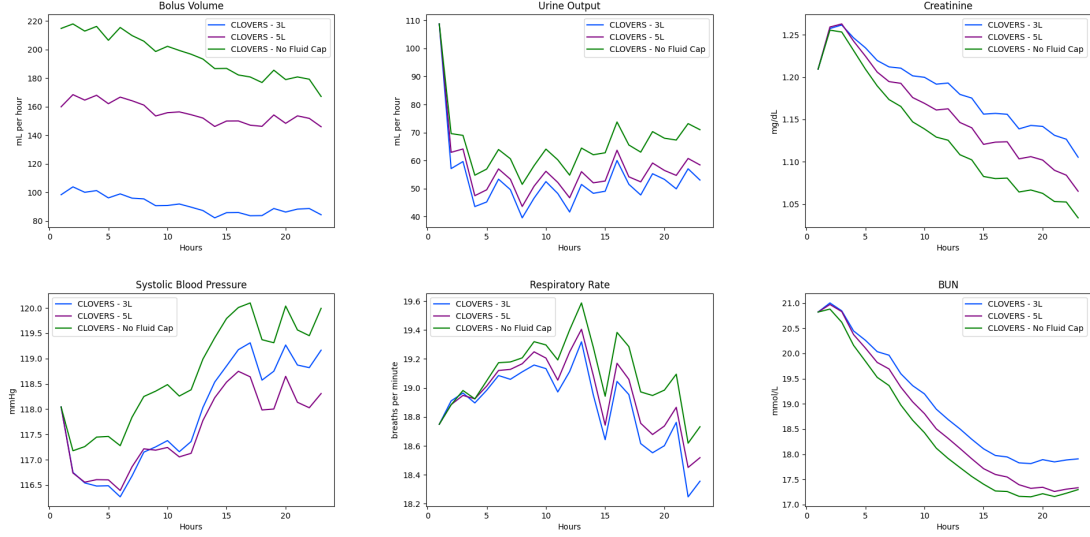


Figure 5: Population-level trajectories under counterfactual fluids strategies. G-Transformer’s predictions for selected covariates under various counterfactual fluids strategies, including two fluids limiting strategies with 3L (blue) and 5L (purple) fluids cap, and a fluids liberal (green) strategy without fluid cap.

Limitations One limitation of this work is that counterfactual predictive density estimates in our experiments do not take into account uncertainty about model parameter estimate. Specifically, given G-Transformer parameters, the distribution of the Monte Carlo simulations produced by g-computation algorithm constitute an estimate of uncertainty about a counterfactual prediction. However, this estimate ignores uncertainty about the G-Transformer parameter estimates themselves. An important area of future work for G-Transformer is adding support for quantification of model uncertainty.

References

Ioana Bica, Ahmed M Alaa, James Jordon, and Mihaela van der Schaar. Estimating counterfactual treatment outcomes over time through adversarially balanced representations. *International Conference on Learning Representations*, 2020a.

Ioana Bica, Ahmed M Alaa, and Mihaela van der Schaar. Time series deconfounder: Estimating treatment effects over time in the presence of hidden confounders. *International Conference on Machine Learning*, 2020b.

E.R. DeLong, D.M. DeLong, and D.L. Clarke-Pearson. Comparing the areas under two or more correlated receiver operating characteristic curves: a nonparametric approach. *Biometrics*, 44:837–845, 1988.

Dennis Frauen, Tobias Hatt, Valentyn Melnychuk, and Stefan Feuerriegel. Estimating average causal effects from patient trajectories. In *Proceedings of the AAAI Conference on Artificial Intelligence*, volume 37, pages 7586–7594, 2023.

C. Geng, H. Paganetti, and C. Grassberger. Prediction of treatment response for combined chemo- and radiation therapy for non-small cell lung cancer patients using a bio-mathematical model. *Scientific Reports*, 2017.

T Heldt, R Mukkamala, GB Moody, and RG Mark. CVSIm: An open-source cardiovascular simulator for teaching and research. *Open Pacing, Electrophysiol & Ther J*, 3:45–54, 2010.

Samuel Holt, Jeroen Berrevoets, Krzysztof Kacprzyk, Zhaozhi Qian, and Mihaela van der Schaar. ODE discovery for longitudinal heterogeneous treatment effects inference. In *The Twelfth International Conference on Learning Representations*, 2024. URL <https://openreview.net/forum?id=pxI5IPeWgW>.

AEW Johnson, L Bulgarelli, L Shen, A Gayles, A Shammout, S Horng, TJ Pollard, B Moody, B Gow, LH Lehman, LA Celi, and RG Mark. MIMIC-IV, a freely accessible electronic health record dataset. *Nature Scientific Data*, 2023a.

Alistair EW Johnson, L Shen, A Gayles, A Shammout, S Horng, TJ Pollard, Benjamin Moody, B Gow, LH Lehman, Leo Anthony Celi, and Roger G Mark. Mimic-iv, a freely accessible electronic health record dataset. *sci data*, 10(1), 2023b.

Rui Li, Stephanie Hu, Mingyu Lu, Yuria Utusumi, Prithwish Chakraborty, Daby Sow, Piyush Madan, Mohamed Ghalwash, Zach Shahn, and Li-wei H Lehman. G-net: a recurrent network approach to g-computation for counterfactual prediction under a dynamic treatment regime. *Proceedings of Machine Learning for Health*, 2021.

Bryan Lim, Ahmed Alaa, and Mihaela Van der Schaar. Forecasting treatment responses over time using recurrent marginal structural networks. In *Neural Information Processing Systems (NIPS)*., 2018.

Ruoqi Liu, Katherine M Hunold, Jeffrey M Caterino, and Ping Zhang. Estimating treatment effects for time-to-treatment antibiotic stewardship in sepsis. *Nature machine intelligence*, 5(4):421–431, 2023.

Valentyn Melnychuk, Dennis Frauen, and Stefan Feuerriegel. Causal transformer for estimating counterfactual outcomes. *arXiv preprint arXiv:2204.07258*, 2022.

L Orellana, A Rotnitzky, and JM Robins. Dynamic regime marginal structuralmean models for estimation of optimal dynamic treatment regimes. *Int J Biostat*, 6(2), 2010.

James Robins. A new approach to causal inference in mortality studies with a sustained exposure period—application to control of the healthy worker survivor effect. *Mathematical Modelling*, 1986.

James Robins. A graphical approach to the identification and estimation of causal parameters in mortality studies with sustained exposure periods. *Journal of Chronic Diseases*, 1987.

Nabeel Seedat, Fergus Imrie, Alexis Bellot, Zhaozhi Qian, and Mihaela van der Schaar. Continuous-time modeling of counterfactual outcomes using neural controlled differential equations. In Kamalika Chaudhuri, Stefanie Jegelka, Le Song, Csaba Szepesvari, Gang Niu, and Sivan Sabato, editors, *Proceedings of the 39th International Conference on Machine Learning*, volume 162 of *Proceedings of Machine Learning Research*, pages 19497–19521. PMLR, 17–23 Jul 2022. URL <https://proceedings.mlr.press/v162/seedat22b.html>.

W.H. Self, M.W. Semler, R. Bellomo, S.M. Brown, B.P. deBoisblanc, and June) Exline M.C. (2018, February 2020. Crystalloid liberal or vasopressors early resuscitation in sepsis (clovers). URL <https://clinicaltrials.gov/ct2/show/NCT03434028>.

Zach Shahn, Nathan I. Shapiro, Patrick D. Tyler, Daniel Talmor, and Li-wei H. Lehman. Fluid-limiting treatment strategies among sepsis patients in the icu: a retrospective causal analysis. *Journal of Critical Care*, 24(62), 2020.

M. Singer, C.S. Deutschman, C.W. Seymour, M. Shankar-Hari, D. Annane, M. Bauer, and et al. The third international consensus definitions for sepsis and septic shock (sepsis-3). *JAMA*, 315(8):801–810, February 2016. doi: <https://doi.org/10.1001/jama.2016.0287>.

Megan Su, Stephanie Hu, Hong Xiong, Elias Baedorf Kassis, and Li-wei H Lehman. Counterfactual sepsis outcome prediction under dynamic and time-varying treatment regimes.

Sarah Taubman, James Robins, Murray Mittleman, and Miguel Hernan. Intervening on risk factors for coronary heart disease: An application of the parametric g-formula. *International journal of epidemiology*, 2009.

Mark Van der Laan, Maya Petersen, and Marshall Joffe. History-adjusted marginal structural models and statically-optimal dynamic treatment regimens. *The international journal of biostatistics*, 2005.

Ashish Vaswani, Noam Shazeer, Niki Parmar, Jakob Uszkoreit, Llion Jones, Aidan N Gomez, Łukasz Kaiser, and Illia Polosukhin. Attention is all you need. *Advances in neural information processing systems*, 30, 2017.

F Wu, G Zhao, Y Zhou, X Qian, E Baedorf-Kassis, and Li-wei H. Lehman. Forecasting treatment outcomes over time using alternating deep sequential models. *IEEE Transactions on Biomedical Engineering*, 2023. doi: 10.1109/TBME.2023.3331298.

Appendix A. Additional CVSim Results

A.1. Alternative G-Transformer Architecture Experiment

Our proposed G-Transformer differs from the traditional Transformer, including the Causal Transformer, in the way it is iteratively trained on time-series data. We concatenated the results of the last time step of each sub-sequence to form a complete prediction sequence for optimization. In contrast, traditional Transformers directly use a sequence-to-sequence framework, shifting the training sequence to obtain the sequence that needs to be predicted. We compared the performance of models implemented with these two training methods on the CVSim dataset, and the results are shown in Table 5.

We can observe that models trained using the sequence-to-sequence approach, including the sequence-to-sequence G-Transformer (Seq2seq G-Transformer) and Causal Transformer, perform notably worse in term of individual-level RMSE compared to proposed G-Transformer in this paper, which uses the iterative training approach. One possible explanation is that during the simulation process, we need to dynamically model the outcomes and treatment variables. This simulation algorithm and our training algorithm share a similar step-by-step approach in term of generating results. Therefore, although both training methods attempt to optimize MSE loss over sequences of the same time step length, our iterative training approach can capture some biases introduced when using predicted outcomes and treatment variables as input for the prediction of next time step, thereby achieving better predictive performance.

Furthermore, as demonstrated in Table 5 and Figure 6, our experiments with the full Transformer architecture variant, the sequence-to-sequence G-Transformer featuring the full Encoder-Decoder architecture (Seq2seq G-Transformer + ED), did not perform as expected, possibly due to overfitting caused by an excessive number of parameters. Particularly over longer time intervals, the large number of parameters introduced by the decoder may have adversely affected the simulation process.

Table 5: CVSim: Counterfactual prediction under g_{c1} . Performance of different variants of G-Transformer in predicting remaining 32-hour patient covariate trajectories based on first 34-hour patient covariate trajectories. Values reported represent the individual-level RMSE between the predicted and counterfactual trajectories. ED stands for using entire Transformer Encoder-Decoder rather than just using Transformer Encoder.

| Model | Individual Level $\text{RMSE}_{g_{c1}}$ |
|-------------------------------|--|
| Seq2seq G-Transformer | 1.550 |
| Seq2seq G-Transformer + ED | 1.935 |
| Causal Transformer | 1.435 |
| Proposed G-Transformer | 1.016 |

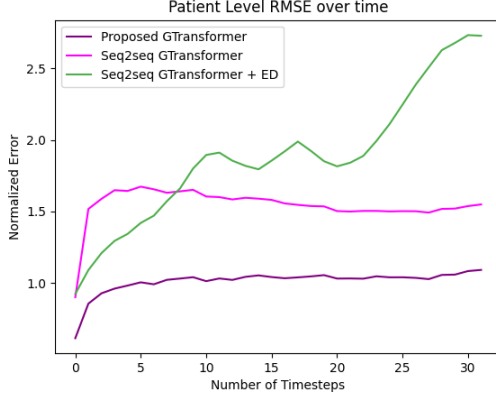


Figure 6: Individual-level RMSE over time under g_{c1} from different variants of G-Transformer

A.2. Gaussian Noise Simulation Experiment

In our proposed G-Transformer Monte Carlo simulation, we sample noise from a distribution of empirical loss from a held-out dataset. Here, we evaluate an alternative approach to sample noise from a normal distribution, with zero mean and empirical covariance estimated from data. As shown in Table 6, sampling noise empirically results in consistently better performance in term of individual-level RMSE across various models when applied to CVSim data under g_{c1} .

Table 6: CVSim: Counterfactual prediction under g_{c1} . Performance of various models with empirical and Gaussian noise sampling in predicting remaining 32-hour patient covariate trajectories based on first 34-hour patient covariate trajectories. Values reported represent the individual-level RMSE between the predicted and counterfactual trajectories.

| Model | Empirical Noise | Gaussian Noise |
|----------------------|-----------------------------------|-----------------------------------|
| | Individual-level RMSE $_{g_{c1}}$ | Individual-level RMSE $_{g_{c1}}$ |
| Linear(g-comp) | 1.103 | 1.418 |
| G-Net | 1.020 | 1.158 |
| G-Transformer | 1.016 | 1.240 |

A.3. Individual-Level RMSE Over Time

Table 7 presents the selected time step-specific individual-level RMSE across different models in CVSim experiment. G-Transformer generally performs better than linear implementation of g-computation and G-Net across the time steps.

Table 7: CVSim: Counterfactual prediction under g_{c1} and g_{c2} . Performance of various models in predicting remaining 32-hour patient covariate trajectories based on first 34-hour patient covariate trajectories per time step. Values reported represent individual-level RMSE between the predicted and counterfactual trajectories.

| | | Linear | GNet | GT |
|----------|----|----------|---------------|--------------|
| | | g-comp | G-Transformer | |
| | | <i>t</i> | | |
| g_{c1} | 1 | 0.688 | 0.654 | 0.615 |
| | 8 | 1.062 | 1.020 | 1.023 |
| | 16 | 1.125 | 1.049 | 1.042 |
| | 24 | 1.168 | 1.052 | 1.047 |
| | 32 | 1.255 | 1.106 | 1.092 |
| g_{c2} | 1 | 0.791 | 0.752 | 0.720 |
| | 8 | 1.122 | 1.079 | 1.077 |
| | 16 | 1.208 | 1.131 | 1.123 |
| | 24 | 1.286 | 1.188 | 1.165 |
| | 32 | 1.348 | 1.213 | 1.186 |

Appendix B. Additional MIMIC Experiments and Results

B.1. Adjustment of Individual-Level RMSE

Individual-level RMSE is adjusted to account for error due to over- and under-prediction in the trajectory length as a result of death and discharge. We use the same technique as in [Su et al.](#) to calculate the individual-level RMSE. Specifically, to account for potential over or under-predictions in trajectory length compared to ground truth, we adopt the following approach to modify the individual-level RMSE calculation. First, for patients who died within the first 24 hours, we replace all subsequent time steps of continuous variables with zero (normalized) until the 24th hour. Covariates with potential negative values are filled with the normalized minimum value in the dataset, while covariates following a log-normal distribution are filled with a normalized logarithmic zero. Second, for patients who were released from the hospital before the end of the first 24 hours in the ICUs, we fill all time steps following hospital release with the population-mean for all continuous variables (up until hour 24). Third, we do the same for the predicted chains (after the predicted death and release outcomes during the first 24 hours) so that all chains have lengths of 24-hours. We then compute the average RMSE across all patients by comparing the predicted trajectory (averaged across 100 Monte Carlo simulations per patient) and the ground-truth trajectory of each patient across all continuous variables.

Appendix C. CVSim Data Generation

A CVSim 6-compartment circulatory model takes as inputs 28 variables that together govern a hemodynamic system. It then deterministically simulates forward in time a set of 25 output variables according to a collection of differential equations (parameterized by the

input variables) modeling hemodynamics. Important variables in CVSIm include arterial pressure (AP), central venous pressure (CVP), total blood volume (TBV), and total peripheral resistance (TPR). In real patients, physicians observe AP and CVP and seek to keep them above a clinically safe threshold. They do this by intervening on TBV (through fluid administration) and TPR (through vasopressors).

We defined simulated treatment interventions that were designed to mimic the impact of fluids and vasopressors. These simulated interventions alter the natural course of the simulation by increasing either TBV (in the case of the simulated fluids intervention) or TPR (in the case of the simulated vasopressor intervention). We generated patients by randomly initiating baseline inputs (which we hid from our G-Nets to make this a stochastic modeling problem) within plausible physiologic ranges, then using CVSIm to simulate covariates forward, intervening according to the relevant treatment strategy at each timestep. Full details of the simulation process can be found in the Appendix.

Under (stochastic) observational treatment strategy g_o , the probability of receiving a non-zero vasopressor or fluid dose at a given time increases as MAP and CVP decrease according to a logistic regression function. Given that a dose is non-zero, the exact amount is drawn from a normal distribution with mean inversely proportional to MAP and CVP. Since all drivers of treatment under g_o are observed in our data, the sequential exchangeability assumption holds and g-computation may be validly applied.

g_{c1} is similar to g_o , except it is a deterministic treatment strategy and the functions linking treatment and dose to covariates have different coefficients. Under g_{c2} , treatment is always withheld.

Appendix D. MIMIC Data and Experiments

Our cohort was limited to ICU stays in which the patient was identified as septic under the Third International Consensus Definitions for Sepsis and Septic Shock (Sepsis-3) [Singer et al. \(2016\)](#). Patients with missing records of pre-ICU fluids or admitted to the ICU following cardiac, vascular, or trauma surgery were removed.

We use AUC to evaluate our 24 hour outcome prediction performance. For each delay k , we do not include patients who have experienced death or release before hour k . A patient is positively labelled if they experience an outcome from hours k to 24. Table 8 presents these test cohort statistics.

Table 8: 24-Hour Cohort Statistics. Size of the test sets used to evaluate AUCs and the respective percent of patients experiencing each outcome from hour k to 24.

| k | Edema | MV | Diuretics | Dialysis | Release | Death |
|----------|---------------|---------------|------------------|-----------------|----------------|--------------|
| 2 | (894, 29.98%) | (894, 40.94%) | (894, 15.10%) | (894, 2.68%) | (894, 13.20%) | (894, 2.35%) |
| 4 | (894, 29.87%) | (894, 40.04%) | (894, 13.87%) | (894, 2.68%) | (894, 13.20%) | (894, 2.35%) |
| 6 | (894, 29.75%) | (894, 38.81%) | (894, 12.75%) | (894, 2.68%) | (894, 13.20%) | (894, 2.35%) |
| 8 | (892, 29.82%) | (892, 36.77%) | (892, 12.22%) | (892, 2.69%) | (892, 13.12%) | (892, 2.24%) |

As predictors to our model, we selected covariates that are typically monitored in the ICU and important for determining sepsis intervention strategies, as well as potential con-

Table 9: MIMIC static variables. All variables were used as inputs to our models.

| Variable Name | Variable Type | Units |
|--------------------------|---------------|-------|
| Age | Continuous | years |
| Gender | Binary | N/A |
| Pre-ICU Fluid Amount | Continuous | mL |
| Elixhauser Score | Continuous | N/A |
| End Stage Renal Failure | Binary | N/A |
| Congestive Heart Failure | Binary | N/A |

founders. The covariates we used were similar to that of Li et al. [Li et al. \(2021\)](#), encompassing, but not limited to, basic demographic information, an Elixhauser comorbidity score, a SOFA score, laboratory values and vital signs, and urine output [Li et al. \(2021\)](#). A comprehensive list is provided in Tables 9 and 10. The demographics, comorbidities, and pre-ICU fluids were unmodeled and regarded as static while the remaining variables were modeled and regarded as dynamic (time-varying).

Appendix E. Hyperparameter Settings

E.1. Settings in Cancer Growth Experiments

Hyperparameter optimization on Cancer Growth data was performed by searching over the hyperparameter space shown in [Table 11](#) with optimal parameters starred. The experiments were performed on NVIDIA Tesla K80 GPU with 12 vCPUs + 110 GB memory. Hyperparameter settings of rMSN and CRN were as reported in [Li et al. \(2021\)](#).

E.2. Settings in CVSim Data

Hyperparameter optimization on CVSim data was performed by searching over the hyperparameter space shown in [Table 12](#) with optimal parameters starred. All models were trained using the Adam optimizer with early stopping with patience of 10 epochs for a maximum of 50 epochs. Also, we utilized the `CosineAnnealingWarmRestarts` scheduler from PyTorch’s optimization module, configured with parameters $T_0 = 10$ and $\text{eta_min} = 0.00001$, to adjust the learning rate following a cosine annealing pattern. The experiments were performed on NVIDIA Tesla T4 GPU with 8 vCPUs + 15GB of dedicated memory.

E.3. Settings in MIMIC Data

Hyperparameter optimization on MIMIC data was performed by searching over the hyperparameter space shown in [Table 13](#) with optimal parameters starred. All models were trained using the Adam optimizer with early stopping with patience of 10 epochs for a maximum of 100 epochs. Also, we utilized the `CosineAnnealingWarmRestarts` scheduler from PyTorch’s optimization module, configured with parameters $T_0 = 10$ and $\text{eta_min} = 0.00001$, to adjust the learning rate following a cosine annealing pattern. The experiments were performed on NVIDIA Tesla T4 GPU with 8 vCPUs + 15GB of dedicated memory.

Table 10: MIMIC time-varying variables. All variables were used as inputs to our models, and boluses and vasopressors were also intervention variables. *Refers to maintenance fluids (not an intervention).

| Variable Name | Variable Type | Units |
|---|-----------------------|------------------|
| Heart Rate | Continuous | beats/min |
| Diastolic Blood Pressure | Continuous | mmHg |
| Systolic Blood Pressure | Continuous | mmHg |
| Mean Blood Pressure | Continuous | mmHg |
| Minimum Mean Blood Pressure | Continuous | mmHg |
| Minimum Change in Mean Blood Pressure from Baseline | Continuous | mmHg |
| Minimum Mean Blood Pressure from Baseline | Continuous | mmHg |
| Minimum Change in Mean Blood Pressure from Previous | Continuous | mmHg |
| Temperature | Continuous | degree C |
| SOFA Score | Treated as Continuous | N/A |
| Change in SOFA Score from Baseline | Treated as Continuous | N/A |
| Change in SOFA Score from Previous | Treated as Continuous | N/A |
| Platelet | Continuous | counts/ 10^9 L |
| Hemoglobin | Continuous | g/dL |
| Calcium | Continuous | mg/dL |
| BUN | Continuous | mmol/L |
| Creatinine | Continuous | mg/dL |
| Bicarbonate | Continuous | mmol/L |
| Lactate | Continuous | mmol/L |
| O2 Requirement Level | Continuous | N/A |
| Change in O2 from Baseline | Continuous | N/A |
| Change in O2 from Previous | Continuous | N/A |
| pO2 | Continuous | mmHg |
| sO2 | Continuous | % |
| spO2 | Continuous | % |
| pCO2 | Continuous | mmHg |
| Total CO2 | Continuous | mEq/L |
| pH | Continuous | Numerical[1,14] |
| Base excess | Continuous | mmol/L |
| Weight | Continuous | kgs |
| Change in Weight | Continuous | kgs |
| Respiratory Rate | Continuous | breaths/min |
| Fluid Volume* | Continuous | mL |
| Urine Output | Continuous | mL |
| Cumulative Edema | Binary | N/A |
| Pulmonary Edema Indicator | Binary | N/A |
| Diuretics Indicator | Binary | N/A |
| Dialysis Indicator | Binary | N/A |
| Mechanical Ventilation Indicator | Binary | N/A |
| Vasopressor Indicator | Binary | N/A |
| Bolus Volume | Continuous | mL |
| In-Hospital Mortality Indicator | Binary | N/A |
| Release Indicator | Binary | N/A |
| Cumulative Fluids | Continuous | mL |
| Fluid Balance in ICU | Continuous | mL |

Table 11: Hyperparameter search space in Cancer Growth experiments.

| | Hyperparameters | Search Range |
|------------------------|-----------------------------------|----------------|
| Linear (g-comp) | Learning Rate | 0.001*, 0.01 |
| G-Net | Number of Layers (Representation) | 1*, 2 |
| | Hidden Dimension (Representation) | 8, 16, 32, 64* |
| | Learning Rate | 0.001, 0.01* |
| G-Transformer | Number of Layers (Continuous) | 1*, 2, 4 |
| | Hidden Dimension (Continuous) | 4, 16, 64* |
| | Number of Layers | 2, 4*, 6 |
| | Hidden Dimension | 32, 64*, 128 |
| | Batch Size | 16*, 32 |
| | Learning Rate | 0.0001 |

Table 12: Hyperparameter search space in CVSIm experiments.

| | Hyperparameters | Search Range |
|------------------------|--------------------------------|--------------|
| Linear (g-comp) | Batch Size | 16 |
| | Learning Rate | 0.0001 |
| G-Net | Number of Layers (Continuous) | 2*, 3 |
| | Hidden Dimension (Categorical) | 64, 128* |
| | Hidden Dimension (Continuous) | 64, 128* |
| G-Transformer | Batch Size | 16 |
| | Learning Rate | 0.0001 |
| | Number of Layers | 3 |
| | Hidden Dimension | 32, 64, 128* |
| | Batch Size | 16 |
| | Learning Rate | 0.0001 |

E.4. Settings for Causal Transformer

Different from the Causal Transformer paper, we did not generate different counterfactual trajectories on the Cancer Growth dataset at each time step using *Single sliding treatment* or *Random trajectories*. For each patient in the test set, we inserted our counterfactual treatment at the last 5 time steps and applied this counterfactual treatment in each subsequent time step. In addition, for multi-step time prediction with Causal Transformer, we predicted the next 4 time steps and $\tau = 5$ in this dataset. In both the CVSIm dataset and the MIMIC dataset, since the model setup does not allow access to the actual treatment, we

Table 13: Hyperparameter search space in MIMIC experiments.

| | Hyperparameters | Search Range |
|----------------------|--------------------------------|--------------|
| G-Net | Number of Layers (Continuous) | 2*, 3 |
| | Hidden Dimension (Categorical) | 64 |
| | Hidden Dimension (Continuous) | 64, 128* |
| | Batch Size | 16 |
| | Weight Decay | 1e-6 |
| | Learning Rate | 0.0001 |
| G-Transformer | Number of Layers | 2*, 3 |
| | Hidden Dimension | 64*, 128 |
| | Batch Size | 16 |
| | Weight Decay | 1e-5 |
| | Learning Rate | 0.0001 |

modified parts of the Causal Transformer’s code to enable the model to use the predicted treatment as input for predicting the outcomes of the next time step.

Hyperparameter Settings For MIMIC and Cancer growth dataset, given that the Causal Transformer has already provided rich information on hyperparameter settings in the original paper (Melnychuk et al., 2022), we used their hyperparameter settings in experiments. For CVSIm dataset, we made slight adjustments to the hidden dimension for experimentation as its format is similar to that of the MIMIC dataset. The specific hyperparameter settings are shown in the table 14.

Table 14: Hyperparameter setting for Causal Transformer in different experiments.

| | Hyperparameters | Search Range |
|----------------------|---------------------------|--------------|
| MIMIC | Dropout rates | 0.2 |
| | Number of Layers | 2 |
| | Number of attention heads | 3 |
| | Number of epochs | 100 |
| | Hidden Dimension | 44 |
| | Learning Rate | 0.001 |
| Cancer Growth | Dropout rates | 0.1 |
| | Number of Layers | 2 |
| | Number of attention heads | 3 |
| | Number of epochs | 150 |
| | Hidden Dimension | 48 |
| | Learning Rate | 0.0001 |
| CVSim | Dropout rates | 0.2 |
| | Number of Layers | 2 |
| | Number of attention heads | 3 |
| | Number of epochs | 100 |
| | Hidden Dimension | 24 |
| | Learning Rate | 0.0001 |